Geometry-induced monopole magnetic field and quantum spin Hall effects

Yong-Long Wang,[1,2,3,*] Hao Zhao,[1,2] Hua Jiang,[1] Hui Liu,[2,†] and Yan-Feng Chen[3,‡]
[1]*School of Physics and Electronic Engineering, Linyi University, Linyi 276000, China*
[2]*Department of Physics, Nanjing University, Nanjing 210093, China*
[3]*National Laboratory of Solid State Microstructures, Department of Materials Science and Engineering, Nanjing University, Nanjing 210093, China*

(Received 27 September 2021; revised 22 November 2022; accepted 28 November 2022; published 5 December 2022)

For a relativistic particle confined to a Möbius strip, the effective Dirac equation is first given in the thin-layer quantization formalism. We find that an effective gauge potential results from the rotation transformation of the adapted frame moving on the Möbius strip, and that an effective mass results from the rescaling transformation determined by the metric tensor of the Möbius strip. It is intriguing that the geometry-induced gauge potential can provide an effective monopole magnetic field for the particle with spin, and can induce quantum spin Hall effects. As potential applications, an effective monopole magnetic field and spin Hall effects can be generated and manipulated by designing the geometry of a two-dimensional nanodevice.

DOI: 10.1103/PhysRevB.106.235403

I. INTRODUCTION

With the rapid development of artificial microstructure technology, theoretical and experimental physicists are trying to investigate novel phenomena of Hall physics in thin films with complex geometries. Those investigations boost the research interest in effective quantum dynamics for two-dimensional (2D) curved systems. A much more suitable scheme, the thin-layer quantization, was primitively employed to study the geometric quantum effects of curved surface by introducing a confining potential [1,2], and then the scheme was extended to a low-dimensional manifold embedded in a high-dimensional manifold [3]. In order to eliminate the ambiguity order, the quantization approach was clearly regularized in a fundamental formalism [4], in which the geometric effects mainly manifest as a scalar geometric potential [2], a geometric momentum [5,6], and a geometric gauge potential [3,7]. The scalar geometric potential was proved to construct a topological band structure for periodically minimal surfaces [8], to generate bound states for spirally rolled-up nanotubes [9], to eliminate the reflection for bent waveguides [10], to provide the transmission gaps for periodically corrugated thin layers [11,12], and so on. It was found that the geometric momentum can contribute [13] and modify the spin-orbit coupling [6,14,15]. As empirical evidences, the scalar geometric potential was realized by an optical analog in a topological crystal [16], and the geometric momentum was demonstrated by the propagation of surface plasmon polaritons on metallic wires [17]. In other words, the thin-layer quantization formalism is valid for low-dimensional curved systems.

To the best of our knowledge, the thin-layer quantization formalism was successfully employed to deduce the effective Schrödinger equation [1,2,18–25] and the effective Pauli equation [26–28]. Most of the known geometric effects are induced by curvature that can be directly determined by the relationship between the three-dimensional (3D) metric tensor and the 2D metric tensor [1,2]. In other words, the curvature-induced effects can be given by a diffeomorphism transformation. As a crucial ingredient, the geometric potential in the nonrelativistic case does not appear in the effective Dirac equation [29–32]. Therefore, for a relativistic particle confined to a curved surface the geometric effects need further investigation. Because the spinor is not a representation of a diffeomorphism group, we have to additionally consider the rotation transformations of dreibein fields that are local Lorentz rotations [33]. In the thin-layer quantization formalism, the effective quantum dynamics is obtained by reducing normal degrees of freedom. Specifically, one finds that the geometric effects can be induced by not only curvature, but also torsion [7]. The torsion-induced effects have been demonstrated in a twisted quantum ring [34,35], on a Möbius ladder [36,37] and a space curve [38] as an effective magnetic moment, a Zeeman-like coupling, and an anomalous phase shift [39], respectively. Therefore, in the torsion-induced gauge structure, the nontrivial properties of geometry-induced magnetic fields and the topological properties of torsion Landau levels need further investigation.

The Dirac magnetic monopole is an Abelian monopole that results from the singularities of an electromagnetic field [40]. Decades later a non-Abelian magnetic field was generalized for the non-Abelian Yang-Mills gauge field [41–43]. Although the magnetic monopole is not an active research topic, the related researches are still published from time to time. Theoretically, the magnetic monopole was constructed in the pure Yang-Mills theory [41], in the Georgi-Glashow model [44], and in the "complementary" gauge-scalar model [45], respectively. Experimentally, the magnetic monopole was realized in bilayer graphene [46,47]. Particularly, the discussions of magnetic monopole were triggered by the appearance of SU(2)

*wangyonglong@lyu.edu.cn
†liuhui@nju.edu.cn
‡yfchen@nju.edu.cn

gauge theory in the classification of four manifolds [48]. In a more general case, the effective quantum dynamics on a 2D manifold or a one-dimensional manifold can be endowed with SU(2) gauge structures by introducing a confining potential with SO(3) symmetries to reduce two degrees of freedom [38,49]. For a specific case, it was proved that the effective dynamics confined to a particular curved surface is endowed with $U(1)$ gauge structure by introducing a confining potential with SO(2) symmetries to reduce one degree of freedom [50]. Mathematically, those Abelian and non-Abelian gauge fields can be induced by the geometry of a curved system as well as that induced by strain [51] or the tensor monopole [52]. As an important result in the present paper, the SU(2) structure of an effective gauge potential can be determined by the geometry of a Möbius strip, and provides an effective monopole magnetic field. For spin [53], the topology of a Möbius strip plays the role of an effective magnetic field.

The quantum spin Hall effect is a new topological state of quantum matter without an applied magnetic field, which is different from the traditional quantum Hall effect with an applied magnetic field. It is striking that the quantum spin Hall effect was primitively and independently predicted as the spin-orbit coupling [54,55] and as the presence of strain gradients [56]. Subsequently, the new topological phenomenon was experimentally realized in HgTe quantum wells [57]. For the quantum Hall effect, the quantized Hall conductances are determined by the quantum Landau levels that are created by applied magnetic fields, while the quantum spin Hall effect is determined by the degenerate quantum Landau levels that are created by the spin-orbit coupling in conventional semiconductors [58,59]. In virtue of that, the geometrical structures of curved systems can provide an effective gauge potential for particles with orbital spin [7,60], it is worthwhile to further investigate the relationship between the nontrivial topology of quantum Hall state [35] and that of a 2D curved surface. As the nontrivial topological states can be constructed by the topology of a Möbius band [35] and the quantum spin Hall effect can be induced by the curvature of a Möbius strip [61].

As previous;y mentioned, we will deduce the effective Dirac equation for a relativistic particle confined to a Möbius strip, and will specifically study the quantum effects induced by the nontrivial properties of a Möbius strip. The present paper is organized as follows. In Sec. II the geometrical properties of a Möbius strip are reviewed. In Sec. III the thin-layer quantization formalism is briefly discussed, and then it is employed to deduce the effective Dirac equation for the relativistic particle confined to a Möbius strip. In Sec. IV we discuss that an effective monopole magnetic field is induced by a torsion, which is the topology of a Möbius strip. In Sec. V we find that quantum spin Hall effects can be induced by the geometry of a Möbius strip, which can be taken as the response of spin to torsion. In Sec. VI the conclusions and discussions are given.

II. THE GEOMETRICAL PROPERTIES OF A MÖBIUS STRIP

For a curved surface $\mathbb{S}^2$, one can adapt a suitable curvilinear coordinate system to describe it as $\mathbf{r}(q_1, q_2)$, a function of q_1 and q_2, where q_1 and q_2 are two tangent coordinate

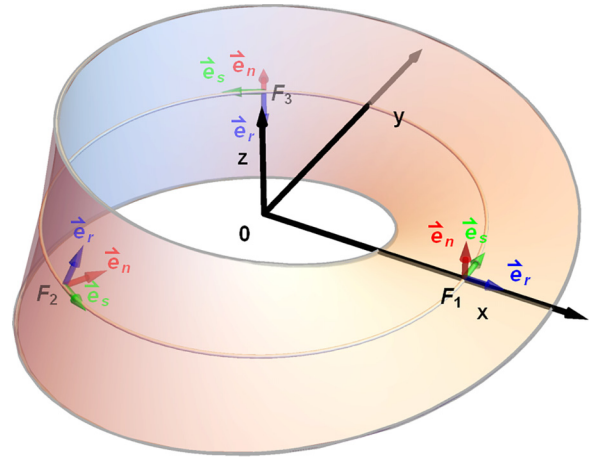

FIG. 1. Schematic of a Möbius strip. $\vec{e}_r$ and $\vec{e}_s$ are two tangent unit basis vectors, and $\vec{e}_n$ is the normal unit basis vector of a Möbius strip. The local frames F_1, F_2, and F_3 are localized at $\theta = 0, \frac{4\pi}{3}, \frac{8\pi}{3}$, respectively.

variables of $\mathbb{S}^2$. For a point near $\mathbb{S}^2$, an additional coordinate variable q_3 normal to $\mathbb{S}^2$ has to be introduced to parametrize as $\mathbf{R}(q_1, q_2, q_3) = \mathbf{r}(q_1, q_2) + q_3\mathbf{n}$, where $\mathbf{n}$ denotes the unit basis vector normal to $\mathbb{S}^2$. The presence of $\mathbb{S}^2$ will deform its near space denoted as $\Xi\mathbb{S}^2$. The deformation can be described by a diffeomorphism transformation that belongs to $GL(3, \mathbb{R})$. As usual, a relativistic particle can be described by a spinor. Without a spinor representation, $GL(3, \mathbb{R})$ cannot be employed to describe the actions of diffeomorphism transformation on the spinor confined to $\mathbb{S}^2$. However, the confined spinor will obey the rotation transformation connecting the local frames at different points on $\mathbb{S}^2$ [62], which is a generator of SO(3). In order to further learn the specific actions of the diffeomorphism transformation and the rotation transformation on the spinor confined to a curved surface in a special case with nonvanishing torsion, we will consider a Möbius strip. In view of the reality, an actually curved surface has a certain thickness. As the scale size of the thickness is small enough, the gap between the ground and first excited normal states would be large enough. In that case, the confined particle will permanently stay at the ground state, and the thin-layer quantization scheme is valid. A Möbius strip of half-width w with a midcircle of radius R and at height $z = 0$ can be parametrized by $\mathbf{r}(r, \theta) = (r_x, r_y, r_z)$ with

$$
\begin{aligned}
r_x(r, \theta) &= \left[R + r\cos\left(\frac{\theta}{2}\right)\right]\cos\theta, \\
r_y(r, \theta) &= \left[R + r\cos\left(\frac{\theta}{2}\right)\right]\sin\theta, \\
r_z(r, \theta) &= r\sin\left(\frac{\theta}{2}\right),
\end{aligned} \tag{1}
$$

where r and θ are two variables with $r \in [-w, w]$ and $\theta \in [0, 4\pi]$, and R can be taken as a constant. The Möbius strip is denoted by $\mathbb{M}^2$ and sketched in Fig. 1. For convenience we adapt an orthogonal frame spanned by two tangent vectors $\mathbf{e}_r$ and $\mathbf{e}_s$ and a normal vector $\mathbf{e}_n$. It is worth noting that the direction of the adapted local frame is moving on $\mathbb{M}^2$.

According to Eq. (1), we can obtain the three basis vectors as

$$\begin{aligned}
\mathbf{e}_r &= \left(\cos\frac{\theta}{2}\cos\theta, \cos\frac{\theta}{2}\sin\theta, \sin\frac{\theta}{2}\right),\\
\mathbf{e}_s &= \frac{2}{N}\Bigg[-\left(R\sin\theta + \frac{3}{2}r\cos\theta\sin\frac{\theta}{2} + r\sin\frac{\theta}{2}\right),\\
&\quad \times R\cos\theta + \frac{1}{4}r\cos\frac{\theta}{2} + \frac{3}{4}r\cos\frac{3\theta}{2}, \frac{1}{2}r\cos\frac{\theta}{2}\Bigg],\\
\mathbf{e}_n &= \frac{2}{N}\Bigg[R\sin\frac{\theta}{2}\cos\theta - r\sin^2\frac{\theta}{2}\sin\theta,\\
&\quad \times R\sin\frac{\theta}{2}\sin\theta + \frac{1}{2}r(\sin^2\theta + \cos\theta),\\
&\quad - R\cos\frac{\theta}{2} - r\cos^2\frac{\theta}{2}\Bigg],
\end{aligned} \tag{2}$$

respectively, where N is a normalized constant as

$$N = \left(4R^2 + 8Rr\cos\frac{\theta}{2} + 2r^2\cos\theta + 3r^2\right)^{1/2}. \tag{3}$$

It is straightforward that $(\mathbf{e}_r, \mathbf{e}_s, \mathbf{e}_n)$ can be obtained by the usual basis vectors $(\mathbf{e}_x, \mathbf{e}_y, \mathbf{e}_z)$ through a rotation transformation $U_{\mathcal{R}}$ in the following form:

$$\begin{bmatrix}\mathbf{e}_r\\ \mathbf{e}_s\\ \mathbf{e}_n\end{bmatrix} = U_{\mathcal{R}}(r,\theta)\begin{bmatrix}\mathbf{e}_x\\ \mathbf{e}_y\\ \mathbf{e}_z\end{bmatrix}, \tag{4}$$

where $U_{\mathcal{R}}$ can be specifically expressed as

$$U_{\mathcal{R}}(r,\theta) = \begin{bmatrix} e_r^x & e_r^y & e_r^z\\ e_s^x & e_s^y & e_s^z\\ e_n^x & e_n^y & e_n^z\end{bmatrix}, \tag{5}$$

through the dreibeins e_α^i $(\alpha = r, s, n)$ and $(i = x, y, z)$, which can be written as

$$\begin{aligned}
e_r^x &= \frac{\partial r_x}{\partial r} = \cos\frac{\theta}{2}\cos\theta,\\
e_r^y &= \frac{\partial r_y}{\partial r} = \cos\frac{\theta}{2}\sin\theta,\\
e_r^z &= \frac{\partial r_z}{\partial r} = \sin\frac{\theta}{2},\\
e_s^x &= \frac{2\partial r_x}{N\partial\theta} = -\frac{1}{N}\left(4R\cos\frac{\theta}{2} + 3r\cos\theta + 2r\right)\sin\frac{\theta}{2},\\
e_s^y &= \frac{2\partial r_y}{N\partial\theta} = \frac{1}{N}\left(2R\cos\theta + \frac{1}{2}r\cos\frac{\theta}{2} + \frac{3}{2}r\cos\frac{3\theta}{2}\right),\\
e_s^z &= \frac{2\partial r_z}{N\partial\theta} = \frac{1}{N}r\cos\frac{\theta}{2},\\
e_n^x &= e_r^y e_s^z - e_r^z e_s^y\\
&= \frac{2}{N}\left(R\sin\frac{\theta}{2}\cos\theta - r\sin^2\frac{\theta}{2}\sin\theta\right),\\
e_n^y &= e_r^z e_s^x - e_r^x e_s^z\\
&= \frac{1}{N}\left[2R\sin\frac{\theta}{2}\sin\theta + r(\sin^2\theta + \cos\theta)\right],\\
e_n^z &= e_r^x e_s^y - e_r^y e_s^x\\
&= -\frac{2}{N}\left(R\cos\frac{\theta}{2} + r\cos^2\frac{\theta}{2}\right).
\end{aligned} \tag{6}$$

It is easy to check that $U_{\mathcal{R}}(r,\theta)$ is a generator of SU(2) group, the universal cover of SO(3), for $\theta \in [0, 4\pi]$.

As an immediate result, the geometry of a Möbius strip will deform its near normal space that can be denoted as $\Xi\mathbb{M}^2$. The deformation will bring the information of normal space into the tangent space, which can be described by a rescaling factor f that relates the 3D metric tensor $G_{\alpha\beta}$ and the 2D metric tensor g_{ab}. With the definition $g_{ab} = \partial_a\mathbf{r}\cdot\partial_b\mathbf{r}$ $(a, b = 1, 2)$, the metric tensor defined on $\mathbb{M}^2$ can be given by

$$g_{ab} = \begin{bmatrix}1 & 0\\ 0 & \frac{N^2}{4}\end{bmatrix}, \tag{7}$$

and the corresponding determinant and the inverse matrix can be obtained as

$$g = \frac{N^2}{4} \tag{8}$$

and

$$g^{ab} = \begin{bmatrix}1 & 0\\ 0 & \frac{4}{N^2}\end{bmatrix}, \tag{9}$$

respectively. With the definition $h_{ab} = \mathbf{e}_n\cdot\partial^2\mathbf{r}/\partial q^a\partial q^b$ $(a, b = 1, 2)$, the second fundamental form h_{ab} can be given by

$$h_{ab} = \begin{bmatrix}0 & R/N\\ R/N & \frac{N^2+r^2}{2N}\sin\frac{\theta}{2}\end{bmatrix}. \tag{10}$$

Furthermore, the Weingarten curvature matrix can be calculated as

$$\alpha_a^b = \begin{bmatrix}0 & -4R/N^3\\ -R/N & -\frac{2(N^2+r^2)}{N^3}\sin\frac{\theta}{2}\end{bmatrix}, \tag{11}$$

with $\alpha_a^b = -h_{ac}g^{cb}$.

In terms of $\mathbb{M}^2$, the position vector of a point in $\Xi\mathbb{M}^2$ can be parametrized by

$$\mathbf{R}(\theta, r, q_3) = \mathbf{r}(\theta, r) + q_3\mathbf{e}_n, \tag{12}$$

where q_3 is the coordinate variable normal to $\mathbb{M}^2$. With the definition $G_{\alpha\beta} = \partial_\alpha\mathbf{R}\cdot\partial_\beta\mathbf{R}$ $(\alpha, \beta = 1, 2, 3)$, the covariant elements G_{ab} can be described as

$$G_{ab} = g_{ab} + (\alpha g + g^T\alpha^T)_{ab}q_3 + (\alpha g\alpha^T)_{ab}(q_3)^2 \tag{13}$$

by g_{ab} and α_a^b, and $G_{33} = 1$ and the rest elements vanish. It is easy to prove that g, the determinant of g_{ab}, and G, the determinant of $G_{\alpha\beta}$, satisfy the following simple relationship:

$$G = f^2 g, \tag{14}$$

where f is the rescaling factor,

$$f = 1 + \mathrm{Tr}(\alpha)q_3 + \det(\alpha)(q_3)^2. \tag{15}$$

The Dirac equation contains only a one-order derivative operator. In the thin-layer quantization formalism, $f^{\frac{1}{2}}$ and $f^{-1/2}$ can be further approximated as

$$f^{\mp 1/2} \approx 1 \mp \tfrac{1}{2}\mathrm{Tr}(\alpha)q_3. \tag{16}$$

Obviously the determinant of α_a^b disappears from Eq. (16). In other words, the geometric effects resulting from the rescaling factor depend only on the mean curvature M of $\mathbb{M}^2$, not on the Gaussian curvature K. M and K can be expressed in the following form:

$$M = \frac{1}{2}\mathrm{Tr}(\alpha) = \frac{(N^2 + r^2)\sin\frac{\theta}{2}}{N^3}, \qquad K = \det(\alpha) = -\frac{4R^2}{N^4}, \tag{17}$$

respectively. However, in the nonrelativistic limit the effective Hamiltonian will contain two-order derivative operators, the factors $f^{1/2}$ and $f^{-1/2}$ have to contain the terms of $(q_3)^2$, and K will then contribute additional geometric effects. As a consequence, in the case of a curved surface with nonzero K, the thin-layer scheme does not commutate with the nonrelativistic limit, the measurement was recently discussed [63].

III. THE EFFECTIVE DIRAC EQUATION ON A MÖBIUS STRIP

In this section, for a relativistic particle confined to $\mathbb{M}^2$, the effective Dirac equation will be given by using the thin-layer quantization scheme. In the semiclassical formalism, a confining potential is first introduced to reduce the degree of freedom normal to $\mathbb{M}^2$. Without loss of generality, the strength of the confining potential cannot be strong enough to create particle and antiparticle pairs [30]. In other words, the number of particles is conserved in the quantization procedure.

A. A rescaling transformation

In quantum mechanics, the particle number conservation can be described by

$$\int |\Psi^\dagger\Psi| d\tau = \int |\Psi|^2\sqrt{G}d^3q = \int |\sqrt{f}\Psi|^2(\sqrt{g}drds)dq_3, \tag{18}$$

where Ψ is a wave function describing a relativistic particle in a usual 3D space, q stands for the three curvilinear coordinate variables, G is the determinant of the metric tensor $G_{\alpha\beta}$ defined in the subspace $\Xi\mathbb{M}^2$, and g is the determinant of the metric tensor g_{ab} defined on the curved surface $\mathbb{M}^2$. The final aim of the thin-layer quantization scheme is to obtain the effective Dirac equation that is separated from the normal component analytically. Notice that the rescaling factor f is in general a function of q_1, q_2, and q_3. The q dependence of G is difficult for the final separation, and which is determined by the diffeomorphism transformation induced by $\mathbb{M}^2$. Specifically, the separation of $\sqrt{G}d^3q$ into a q_3-dependent part and a q_3-independent part can be accomplished by introducing a new wave function χ, $\chi = \sqrt{f}\Psi$, which can eliminate f from $\sqrt{G}d^3q$.

Under the diffeomorphism transformation, the wave function Ψ and an ordinary physical operator $\hat{O}$ satisfy the following transformations:

$$\chi = f^{1/2}\Psi, \qquad \hat{O}' = f^{1/2}\hat{O}f^{-1/2}, \tag{19}$$

where f is the rescaling factor that is defined in Eq. (15). In view of the original intention of the introduction of χ, the above transformation can describe the redistribution of the spatial probability of a particle near $\mathbb{M}^2$. However, this transformation cannot describe well the geometry-induced effects on a spinor. As a consequence, for the spinor on $\mathbb{M}^2$, one has to consider the rotation transformations defined by the background dreibein fields of the Möstrip $\mathbb{M}^2$.

B. A frame rotation transformation

In contrast to the particle described by the Schödinger equation, the particle described by the Dirac equation has an additional intrinsic degree of freedom, spin. Since the spinor is not a representation of $GL(3,\mathbb{R})$, the diffeomorphism transformation cannot describe well the dynamics of a spinor on $\mathbb{M}^2$. As usual, in $\Xi\mathbb{M}^2$ the spinor is taken as the eigenstate of σ_3, where σ_3 is a Pauli matrix. It is easy to check that the basis vectors $(\mathbf{e}_r, \mathbf{e}_s, \mathbf{e}_n)$ can be obtained by $(\mathbf{e}_x, \mathbf{e}_y, \mathbf{e}_z)$ through a rotation transformation $U_\mathcal{R}$, which connects the local frames at different points of $\mathbb{M}^2$. Specifically, σ_3 can be also obtained by σ_z through the rotation transformation $U_\mathcal{R}$. In the Pauli-Dirac representation, for the spinor on $\mathbb{M}^2$, the new wave function χ and the rescaled physical operator $\hat{O}'$ specifically satisfy the following transformations:

$$\chi' = U_\mathcal{R}\chi, \qquad \hat{O}'' = U_\mathcal{R}\hat{O}'U_\mathcal{R}^{-1}, \tag{20}$$

where $U_\mathcal{R}$ is the rotation transformation connecting $(\mathbf{e}_r, \mathbf{e}_s, \mathbf{e}_n)$ and $(\mathbf{e}_x, \mathbf{e}_y, \mathbf{e}_z)$, and $U_\mathcal{R}^{-1}$ is the inverse of $U_\mathcal{R}$.

As a conclusion, for a spinor on $\mathbb{M}^2$, the wave function Ψ and an ordinary physical operator $\hat{O}$ in general satisfy the following transformations:

$$\Psi' = U_\mathcal{R}f^{1/2}\Psi, \qquad \hat{O}' = U_\mathcal{R}f^{1/2}\hat{O}f^{-1/2}U_\mathcal{R}^{-1}, \tag{21}$$

where f is the rescaling factor with the form of Eq. (15) and $U_\mathcal{R}$ is the rotation transformation describing the adapted frame moving on $\mathbb{M}^2$. Furthermore, the effective physical operator describing the spinor confined on $\mathbb{M}^2$ can be given by

$$\hat{O}_{\mathrm{eff}} = \lim_{q_3\to 0}\left(U_\mathcal{R}f^{1/2}\hat{O}f^{-1/2}U_\mathcal{R}^{-1}\right) - \hat{O}_\perp, \tag{22}$$

where $\hat{O}_\perp$ is the normal component of $\hat{O}$. This equation is a key result in the present paper, which condenses the initial spirit of the thin-layer quantization scheme [4]. Interestingly, it is can be extended to vector fields, such as an electromagnetic field [13].

C. Effective Dirac equation

In the spirit of a thin-layer quantization scheme, a relativistic particle is initially described by a usual Dirac equation, that is

$$(i\gamma^\mu\partial_\mu - m)\Psi = 0, \tag{23}$$

where ∂_μ is a derivative operator in (3+1)-dimensional spacetime, m is the static mass of a particle, and γ^μ $(\mu = 0, 1, 2, 3)$

are the 4×4 Dirac matrices that satisfy the following anticommutation relationship:

$$[\gamma^\mu, \gamma^\nu]_+ = \gamma^\mu\gamma^\nu + \gamma^\nu\gamma^\mu = 2\eta^{\mu\nu}, \tag{24}$$

where $\eta^{\mu\nu} = \mathrm{diag}(1, -1, -1, -1)$. In Eq. (23), Ψ is a four-component spinor, which can be separated into a scalar component ψ and a vector component $\hat{s}$ under the transformations Eqs. (19) and (20). In the Pauli-Dirac representation, the Dirac matrices γ^μ can be given by

$$\gamma^0 = \begin{pmatrix} I & 0 \\ 0 & I \end{pmatrix}, \quad \gamma^i = \begin{pmatrix} 0 & \sigma^i \\ -\sigma^i & 0 \end{pmatrix}, \tag{25}$$

where I is a unit 2×2 matrix, and σ^i $(i = x, y, z)$ stand for three Pauli matrices:

$$\sigma^x = \begin{pmatrix} 0 & 1 \\ 1 & 0 \end{pmatrix}, \quad \sigma^y = \begin{pmatrix} 0 & -i \\ i & 0 \end{pmatrix}, \quad \sigma^z = \begin{pmatrix} 1 & 0 \\ 0 & -1 \end{pmatrix}, \tag{26}$$

respectively.

For a relativistic particle in $\Xi\mathbb{M}^2$, one can adapt a local frame, in which the four-component wave function Ψ and the Dirac Hamiltonian H in Eq. (23) should be replaced by a new wave function χ and a new Hamiltonian H' that can be expressed as

$$\begin{aligned} \chi &= U_\mathcal{R} f^{1/2} \Psi, \\ H' &= U_\mathcal{R} f^{1/2} H f^{-1/2} U_\mathcal{R}^{-1}. \end{aligned} \tag{27}$$

Subsequently, a confining potential is introduced to reduce the normal degree of freedom. In the presence of an introduced potential, the relativistic particle is going to stay a long time at the ground normal state of $\mathbb{M}^2$. With the ground normal state and Eq. (22), the effective Dirac Hamiltonian can be specifically determined by

$$\begin{aligned} H_{\mathrm{eff}} &= \lim_{\varepsilon \to 0} \langle \chi_{\perp_0} | \left(U_\mathcal{R} f^{1/2} H f^{-1/2} U_\mathcal{R}^{-1} \right) - H_\perp | \chi_{\perp_0} \rangle \\ &= \langle \chi_{\perp_0} | \left(U_\mathcal{R} f^{1/2} H f^{-1/2} U_\mathcal{R}^{-1} \right) - H_\perp | \chi_{\perp_0} \rangle_0, \end{aligned} \tag{28}$$

where ε describes the scaling size of a normal degree of freedom, and $\chi_{\perp_0}$ is the ground normal state. In order to obtain the solution of ground state, the transformed wave function χ has to be divided into a tangent part $\chi_{\|}(r, s)$ and a normal part $\chi_\perp(q_3)$ as

$$\chi(q) = \chi_\perp(q_3)\chi_\|(r, s). \tag{29}$$

In the process, the time dimension is conveniently taken as a constant variable, and the confining potential cannot be strong enough to create particle and antiparticle pairs [30] to conserve the particle number. For the sake of simplicity, the confining potential V_c can be chosen [64] as an infinitely deep potential well in the following form:

$$V_c = \lim_{\varepsilon \to 0} \begin{cases} 0, & -\frac{\varepsilon}{2} \leqslant q_3 \leqslant \frac{\varepsilon}{2}, \\ \infty, & q_3 < -\frac{\varepsilon}{2}, \quad q_3 > \frac{\varepsilon}{2}, \end{cases} \tag{30}$$

where ε describes the width of the potential well. And the Dirac equation (23) can be rewritten into

$$(i\gamma^\alpha \partial_\alpha - m + V_c)\Psi = E\Psi, \tag{31}$$

where $\alpha = 1, 2, 3$ describes the three coordinate variables of the adapted frame, and E is the eigenenergy.

For the extreme limit of V_c, the normal component of Dirac equation can be directly given as

$$(i\gamma^3 \partial_3 + V_c)\chi_\perp = E_\perp \chi_\perp, \tag{32}$$

where $E_\perp$ is the normal component of energy that satisfies $E_\| + E_\perp = E$, wherein $E_\|$ is the tangent component of energy. In the presence of V_c, the Dirac particle is strictly confined in the interval $[-\varepsilon/2, \varepsilon/2]$, and thus Eq. (32) can be simplified as

$$i\gamma^3 \partial_3 \chi_\perp = E_\perp \chi_\perp. \tag{33}$$

Without spin, the above equation can be further simplified and formed as

$$-\partial_3^2 \chi_\perp = E_\perp^2 \chi_\perp. \tag{34}$$

With the boundary continuous conditions, the specific solution of $\chi_\perp$ can be easily solved as

$$\chi_\perp(q_3) = \sqrt{\frac{2}{\varepsilon}} \cos(k_n q_3), \tag{35}$$

where k_n is the normal component of momentum quantized as $k_n = (2n + 1)\pi/\varepsilon$. With the limit $\varepsilon \to 0$, the gap between the ground state and the first excited state becomes large enough, the Dirac particle will permanently stay in the ground state $|\chi_{\perp 0}\rangle$.

In the Pauli-Dirac representation, the spinor on $\mathbb{M}^2$ can be taken as the eigenstates of σ_3, where σ_3 is a Pauli matrix in the adapted frame. Based on the previous discussions, the new Dirac matrices γ^α and the new derivative operators D_α can be described by the usual Dirac matrices γ^i and the usual derivative operators ∂_i through a rotation transformation $U_\mathcal{R}$,

$$\begin{aligned} \gamma^\alpha &= U_\mathcal{R} \gamma^i = e^\alpha{}_i \gamma^i \\ &= \begin{bmatrix} 0 & \sum_{i=x,y,z} e^\alpha{}_i \sigma^i \\ -\sum_{i=x,y,z} e^\alpha{}_i \sigma^i & 0 \end{bmatrix}, \\ D_\alpha &= U_\mathcal{R}^{-1} \partial_i + \partial_i \left(U_\mathcal{R}^{-1} \right) = e^i_\alpha \partial_i + \left(\partial_i e^i{}_\alpha \right). \end{aligned} \tag{36}$$

Practically, the rotation transformation $U_\mathcal{R}$ can be accomplished by performing three rotation transformations U_z, U_y, and U_x in turn, where U_z is a rotation around $\mathbf{e}_z$, U_y is a rotation around $\mathbf{e}'_y$ that stands for the y axis rotated by U_z, and U_x is a rotation around $\mathbf{e}''_x$ that stands for the x axis rotated by performing U_z and then U_y. In the Cartesian coordinate system, U_z is

$$U_z(\theta) = \begin{bmatrix} \cos\theta & \sin\theta & 0 \\ -\sin\theta & \cos\theta & 0 \\ 0 & 0 & 1 \end{bmatrix}, \tag{37}$$

U_y is

$$U_y(\theta) = \begin{bmatrix} \cos\frac{\theta}{2} & 0 & -\sin\frac{\theta}{2} \\ 0 & 1 & 0 \\ \sin\frac{\theta}{2} & 0 & \cos\frac{\theta}{2} \end{bmatrix}, \tag{38}$$

and U_x is

$$U_x(r, \theta) = \begin{bmatrix} 1 & 0 & 0 \\ 0 & \cos\theta_x & \sin\theta_x \\ 0 & -\sin\theta_x & \cos\theta_x \end{bmatrix}, \tag{39}$$

respectively, here $\cos\theta_x = 2(R + r\cos\frac{\theta}{2})/N$ and $\sin\theta_x = r/N$. It is easy to prove that $U_{\mathcal{R}} = U_x U_y U_z$. In the presentation of σ_3, $U_{\mathcal{R}}$ can be reexpressed as

$$U_{\mathcal{R}}(r,\theta) = e^{-i\boldsymbol{\theta}\cdot\boldsymbol{\sigma}}, \tag{40}$$

where $\boldsymbol{\theta} = (\theta_x, \theta_y, \theta_z)$ and $\boldsymbol{\sigma} = \boldsymbol{e}_n\sigma_3$, with $\theta_x = \arcsin(r/N)$, $\theta_y = \theta/2$, $\theta_z = \theta$.

Substituting Eqs. (16), (35), and (40) into Eq. (28), we can obtain the effective Hamiltonian H_{eff} that describes the relativistic particle confined to $\mathbb{M}^2$ as

$$H_{\text{eff}} = i\gamma^a(\partial_a - i\sigma_3\mathcal{A}_a) - (m + m_{\text{eff}}), \tag{41}$$

where σ_3 just takes its eigenvalues $\sigma_3 = \pm 1$, $\mathcal{A}$ is a geometric gauge potential with $\mathcal{A}_a = \partial_a(\boldsymbol{\theta}\cdot\boldsymbol{\sigma})$ $(a = r, s)$, and m_{eff} is an effective mass induced by the geometry of $\mathbb{M}^2$, $m_{\text{eff}} = \frac{1}{2}\text{Tr}(\alpha)$, wherein α is the Weingartein curvature matrix. For Eq. (41), the effective Dirac equation can be written as

$$[i\gamma^a(\partial_a - i\sigma_3\mathcal{A}_a) - (m + m_{\text{eff}})]|\chi_\parallel\rangle = E_\parallel|\chi_\parallel\rangle, \tag{42}$$

where $E_\parallel$ is the tangent component of eigenenergy, and $|\chi_\parallel\rangle$ stands for the tangent part of the wave function. Strikingly, the geometry of $\mathbb{M}^2$ plays the role of gauge potential for the spinor and the mean curvature of $\mathbb{M}^2$ contributes an effective mass.

Obviously the geometric gauge potential $\mathcal{A}_a$ is given by ∂_a acting on ${U_{\mathcal{R}}}^{-1}$, and the effective mass m_{eff} results from the action of ∂_3 on $f^{-1/2}$. It is worth noting that all the high order terms of q_3 in $f^{-1/2}$ vanishes by performing the integral $\langle\chi_{\perp_0}|\chi_{\perp_0}\rangle_0$. Meaning, the high power terms are losing the actions of ∂_3 before performing the nonrelativistic limit. In other words, the thin-layer quantization scheme does not commute with the nonrelativistic limit process. Importantly, the effective Pauli equation on $\mathbb{M}^2$ should be performed in a certain order [4]. Specifically, the nonrelativistic limit is prior to the thin-layer quantization scheme.

IV. GEOMETRY-INDUCED MONOPOLE MAGNETIC FIELD

The rotation $U_{\mathcal{R}}$ describes the connection of the local frames at different points on $\mathbb{M}^2$, which can be described by two tangent coordinate variables r and s of $\mathbb{M}^2$ without the normal coordinate variable q_3. It is easy to obtain that the three components of the geometric gauge potential are $\mathcal{A}_r = 2R/N^2$,

$$\mathcal{A}_s = \frac{1}{\sqrt{N^2 - r^2}}\sin^2\frac{\theta}{2}\sin^2\theta_x\left(\cos\theta\cos^2\theta_x + \cos\frac{\theta}{2}\sin 2\theta_x\right) + \frac{1}{N}\left[\left(\sin\theta\sin\frac{\theta}{2} + 2\cos\frac{\theta}{2}\right)\cos\theta_x - \cos\theta\sin\theta_x\right], \tag{43}$$

and $\mathcal{A}_n = 0$, respectively. And the geometry-induced magnetic field can be then obtained by

$$\mathcal{B}_n = \partial_r\mathcal{A}_s - \partial_s\mathcal{A}_r \tag{44}$$

and $\mathcal{B}_r = \mathcal{B}_s = 0$, because $\mathcal{A}_r$ and $\mathcal{A}_s$ do not depend on the coordinate variable q_3 and $\mathcal{A}_3 = 0$. Therefore, the geometry-induced magnetic field $\mathcal{B}$ is along the negative normal dimension of $\mathbb{M}^2$ that is sketched in Fig. 2(a) as an effective monopole magnetic field. The result is described in Fig. 2(b). Apparently, the geometry-induced magnetic field always orientates to $\mathbb{M}^2$. The particular monopole magnetic field just appears in the case of a half-integer linking number [65] $\frac{1}{2\pi}\int\tau d\theta = n + \frac{1}{2}$ $(n \in Z)$, with Z being an integer. In the half-integer case, by performing one tour on $\mathbb{M}^2$, one arrives at an opposite magnetic field at the opposite side of $\mathbb{M}^2$ at the same position. Therefore, the geometry-induced magnetic field has a source at $\mathbb{M}^2$. For an integer linking number $\frac{1}{2\pi}\int\tau d\theta = n + 1$, the effective magnetic field becomes an ordinary magnetic field which is sketched in Fig. 2(c), and also projected onto a sphere described in Fig. 2(d). In the integer case, the geometry-induced magnetic field is ordinary with free sources at $\mathbb{M}^2$. The blue arrows denote the effective magnetic field whose direction is determined by the adapted frame moving on one side of $\mathbb{M}^2$. The red arrows stand for the effective magnetic field whose direction is defined by the adapted frame moving on the other side of $\mathbb{M}^2$ in an opposite normal direction. In the blue and red cases, by performing one tour on $\mathbb{M}^2$ with an integer linking number, one arrives at the same magnetic field at the same side of $\mathbb{M}^2$. As a consequence, the effective monopole magnetic field is completely determined by the topology of $\mathbb{M}^2$. And the geometry-induced magnetic field $\mathcal{B}_n$ is specifically described in the plane spanned by r and θ as sketched in Fig. 3.

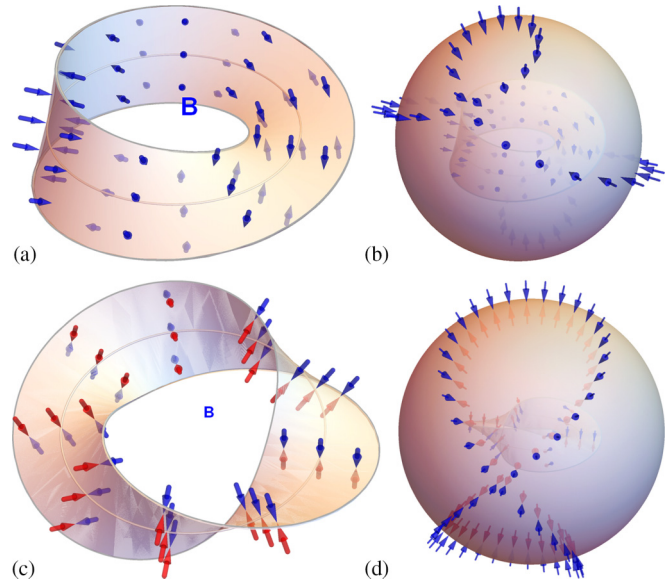

FIG. 2. (a) In the case of a half-integer linking number, there is an effective monopole magnetic field $\boldsymbol{B}$ that is described by blue arrows. The deep blue and light blue arrows denote the magnetic fields on the visible and hidden parts of $\mathbb{M}^2$. (b) The monopole field is projected onto a sphere. (c) In the case of an integer linking number, there is an effective ordinary magnetic field. The blue and red arrows are employed to distinguish the effective ordinary magnetic fields at the different sides of $\mathbb{M}^2$ with opposite normal directions. The deep color and light color arrows denote the magnetic fields on the visible and hidden parts of $\mathbb{M}^2$. (d) The ordinary field is projected onto a sphere.

Noticeably, the geometry-induced magnetic field is distinctly different from the usual magnetic field. The geometry-induced magnetic field acts on a particle by coupling with

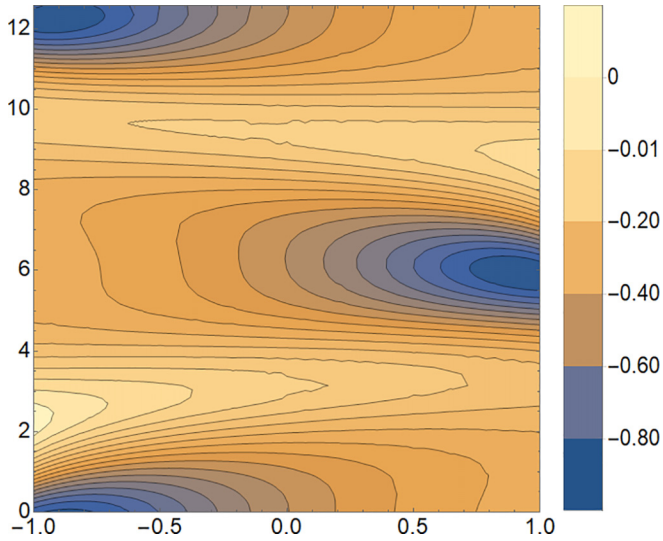

FIG. 3. The contours of a geometry-induced magnetic field in the plane spanned by r and θ with $R = 4$, $r \in [-1, 1]$ and $\theta \in [0, 4\pi]$.

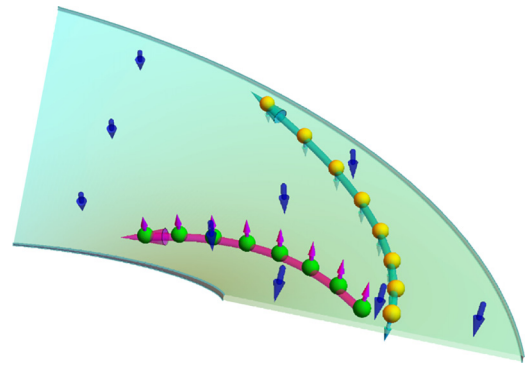

FIG. 4. Schematic of a spin Hall effect on a part of a Möbius strip. The blue arrows denote the geometry-induced magnetic field, the green balls with pink upward arrows are the electrons of spin up, the yellow balls with cyan downward arrows are the electrons of spin down, and the big pink arrow and the big cyan arrow stand for the moving directions of electrons.

spin, while the usual magnetic field acts on a particle by coupling with electric charge. Specifically, the effective magnetic field is determined by the geometries of $\mathbb{M}^2$, and the nontrivial monopole properties are defined by the nontrivial topological properties of $\mathbb{M}^2$. Once the nontrivial single side vanishes, the nontrivial monopole will disappear and an effective ordinary magnetic field will appear. Furthermore, the geometry-induced magnetic field is a non-Abelian gauge field, in general $U_{\mathcal{R}}(\boldsymbol{\theta}_1)U_{\mathcal{R}}(\boldsymbol{\theta}_2) \neq U_{\mathcal{R}}(\boldsymbol{\theta}_2)U_{\mathcal{R}}(\boldsymbol{\theta}_1)$, which determines the gauge structure of the effective Hamiltonian confined on $\mathbb{M}^2$. Under a rotation transformation $U_{\mathcal{R}}(\theta)$, the geometric gauge potential $\mathcal{A}$ and the tangent component of wave function $|\chi_{\parallel}\rangle$ transform as an SU(2) gauge transformation,

$$|\chi_{\parallel}\rangle \to U_{\mathcal{R}}(\theta)|\chi_{\parallel}\rangle,$$
$$\mathcal{A}_t \to U_{\mathcal{R}}(\theta)\mathcal{A}_t U_{\mathcal{R}}^{-1}(\theta) + U_{\mathcal{R}}(\theta)\partial_t U_{\mathcal{R}}^{-1}(\theta), \tag{45}$$

where $t = r, s$ stand for the two tangent component of geometric gauge potential $\mathcal{A}$. In other words, the gauge structure of effective dynamics can be constructed by the geometry of a curved surface. As potential applications, the effective gauge field can be generated and manipulated by designing the geometry of a 2D nanodevice.

V. GEOMETRY-INDUCED QUANTUM SPIN HALL EFFECT

In the presence of $\boldsymbol{A}$, the Dirac particle moving on $\mathbb{M}^2$ will feel a pseudo-Lorentz force induced by the geometry of $\mathbb{M}^2$. Because the spin of the particle initially couples with the geometry of $\mathbb{M}^2$ to contribute the term $\sigma_3\mathcal{A}$ in Eq. (42) [50], which plays the role of spin-orbit coupling [54] in a conventional semiconductor. The effective coupling can be given by a strain gradient [56], and can be partially replaced by another [66]. The geometry-induced coupling can be rewritten into the form $u_3\mathcal{B}_n$ in the nonrelativistic limit, where u_3 denotes the normal component of a spin magnetic moment. According to the left-hand rule, for a certain section of $\mathbb{M}^2$ the spin-out particles gather to one side, the spin-in particles aggregate toward the other side, which are sketched in Fig. 4. The spin-out means that the spin orientation is the normal direction of $\mathbb{M}^2$, while the spin-in means that the spin orientation is the negative normal direction of $\mathbb{M}^2$. As a result, on $\mathbb{M}^2$ the spin-out particles and the spin-in particles are completely separated into two groups, they are gathering on the two sides for a specific section, respectively, and they are collecting on two different faces for a specific edge, respectively. Most strikingly, the spin-in particles and the spin-out particles are moving in the same direction with the same spin polarization as a full spin current for the specific edge that is sketched in Fig. 5(a). Interestingly, the spin polarization is entirely determined by the nontrivial topology of $\mathbb{M}^2$, which determines the degeneracy of pseudo-Landau levels in momentum space. The twofold pseudo-Landau levels are separated by the width of $\mathbb{M}^2$ in configuration space. Mathematically, the Möbius strip is a 2D compact manifold with a single boundary and a one-sided surface. In other words, the topological structure of $\mathbb{M}^2$ can spontaneously flip the "spin-down" into the "spin-up" to provide a pure spin current. For a half-integer number $\frac{1}{2\pi}\oint \tau ds = n + \frac{1}{2}$ $(n \in \mathbb{Z})$, the pure spin current is contributed by a combination of spin-out particles and spin-in particles. In the case of $\frac{1}{2}$, the big cyan arrows and the big pink ones contribute equally to the spin current along the same edge as sketched in Fig. 5(a). In the case of an integer number $\frac{1}{2\pi}\oint \tau ds = n$, the pure spin current is contributed by one type of particle, either the spin-out or the spin-in. The result is sketched in Fig. 5(b) in the presence of the effective magnetic field described by blue arrows as in Fig. 2(c). Distinguishingly, the spin-out particles and the spin-in ones do not have the same contribution to the spin current, and they are impossibly along the same edge. For the effective magnetic field denoted by the red arrows in Fig. 2(c), the same spin polarization will appear on the other side of $\mathbb{M}^2$. The spin polarization is also completely induced by the geometry of $\mathbb{M}^2$ with an integer linking number.

As a classical analogy, this can be thought of in terms of the magnus effect, a spinning soccer ball will "stray" from its normal straight path in a direction dependent on its sense of

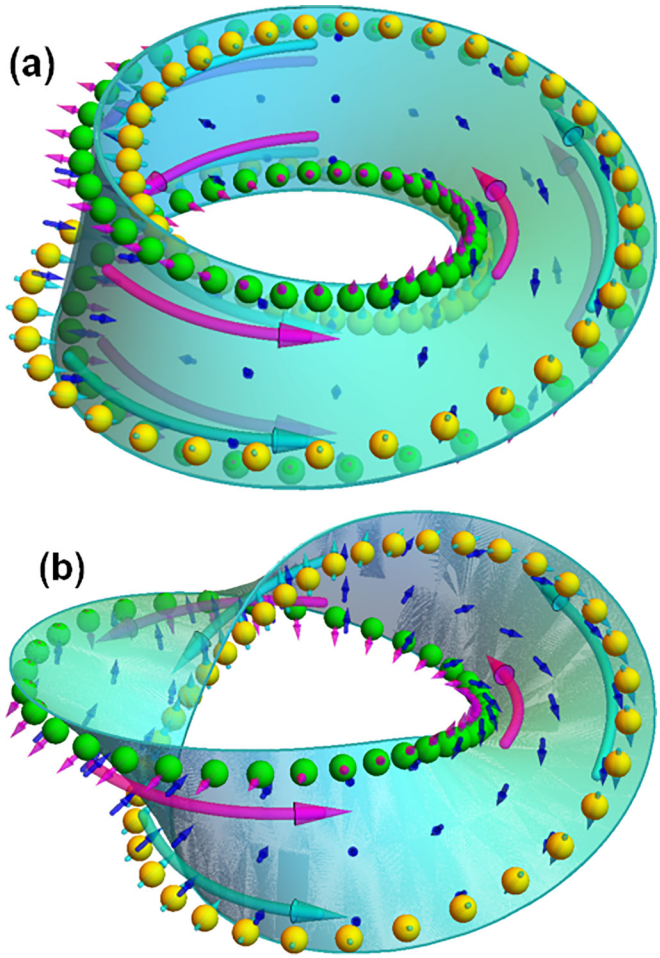

FIG. 5. (a) Spin Hall effect on the Möbius strip of a half-integer linking number $\frac{1}{2}$. (b) Spin Hall effect on the Möbius strip of an integer linking number 1. The blue arrows stand for the geometry-induced magnetic field, the green balls with pink outward arrows denote the spin-out particles, and the yellow balls with cyan inward arrows are the spin-in particles. The big pink arrows stand for the current consisting of spin-out particles, and the big cyan arrows stand for the current consisting of the spin-in ones.

rotation. Therefore, the spin-out particles will initially gather toward one side, while the spin-in ones aggregate toward the other side for a specific section of $\mathbb{M}^2$. In the case of the half-integer linking number, the "so-called" two edges are really the same one. The emergence of quantum spin Hall effect is eventually determined by the geometry of $\mathbb{M}^2$. In the case of an integer linking number, the two edges are completely different, the spin current vanishes for the whole of $\mathbb{M}^2$, and the spin-out current emerges along one edge, while the spin-in current emerges along the other. For the adapted frame moving on different sides of $\mathbb{M}^2$, the spin-out and spin-in currents have the same amplitude. The result agrees well with that given by Ref. [35].

VI. CONCLUSIONS AND DISCUSSIONS

For the quantum particles confined to a 2D curved system, the geometric effects are a long-standing interesting topic. The required effective dynamics can be given by using the thin-layer quantization scheme, which is valid. Because the two important geometric effects, the geometric potential and the geometric momentum, have been proved by experiments. The two effects both result from the rescaling factor that is a function of the normal coordinate variable. The dependence of normal space directly originates from the metric tensor defined in the 3D subspace spanned by the two tangent coordinate variables and the normal variable of $\mathbb{M}^2$. So far, the fundamental framework of the thin-layer quantization scheme is suitable and sufficient for the geometric potential and geometric momentum [2,5,6]. Unfortunately, the fundamental formalism cannot give the geometric gauge potential that is related to the symmetries of the introduced confining potential [7] for the curved surface embedded in the 3D Euclidean space [50]. In order to remove the difficulty, the formula of geometric effects are rediscussed, which is clearly evidenced by the geometric effects that are not only from the rescaling transformation, but also from the rotation transformation intimately connected to the local frames. These results will enable the thin-layer quantization formalism to play a more important and effective role in the effective quantum dynamics for the particles confined to low-dimensional curved systems.

For the particles confined to a Möbius strip, the effective Dirac equation is given by using the developed thin-layer quantization formalism. There are two important results from the geometric effects. One is the effective mass that results from the rescaling factor. The other is the effective gauge potential that results from the rotation transformation connected to the local frames. The presence of the rescaling factor determines that the thin-layer quantization formalism does not commute with the nonrelativistic limit. Interestingly, the effective magnetic field that is determined by the single face of a Möbius strip is monopole. This result provides a feasible way to generate a non-Abelian monopole magnetic field, and the gauge structure can be constructed by designing the geometry of a low-dimensional curved system. In the presence of a monopole effective magnetic field, the spin-out particles and the spin-in ones are completely separated as a full spin polarization. The pure spin current is also determined by the geometry of a Möbius strip due to the coupling of geometry and spin. As a conclusion, the nontrivial topological properties of a Möbius strip entirely determine the emergences of the monopole magnetic field and the quantum spin Hall effect. In other words, the complex geometries and topologies of 2D systems can provide a new perspective to investigate new phenomena of Hall physics implied in a high-dimensional space.

With the rapid development of flexible electronics, flexible spintronics, and metastructure physics, the geometric quantum effects play a more and more important role in the effective quantum dynamics for 2D curved systems. As the considered example, a nanodevice with a Möbius strip can be constructed from the twisted particular lattice strips with domain walls [67], in which one can use multiple domain walls to obtain various higher quantized conductance plateaus. For a monolayer graphene Möbius strip, a geometry-induced spin Hall effect can be observed [61]. And in rf circuits emulating the Möbius strip, the spin flip can be also observed in the

measurements of time-resolved dynamics [68]. Therefore, the geometries of nanodevices can be employed to improve the development of nanodevices and topological quantum computation and topological quantum commutation. Altogether, our results demonstrate a viable manner to control the electronic levels and transpose properties of 2D curved systems, shedding new light on the design of novel electronics devices by geometry engineering.

ACKNOWLEDGMENTS

This work is jointly supported by the Natural Science Foundation of Shandong Province of China (Grant No. ZR2020MA091), the National Key R&D Program of China (Grant No. 2017YFA0303702), the National Nature Science Foundation of China (Grant No. 11625418), and National Lab of Solid State Microstructure of Nanjing University (Grants No. M35040 and No. M35053).

[1] H. Jensen and H. Koppe, Ann. Phys. **63**, 586 (1971).
[2] R. C. T. da Costa, Phys. Rev. A **23**, 1982 (1981).
[3] P. Schuster and R. Jaffe, Ann. Phys. **307**, 132 (2003).
[4] Y.-L. Wang and H.-S. Zong, Ann. Phys. **364**, 68 (2016).
[5] Q. H. Liu, L. H. Tang, and D. M. Xun, Phys. Rev. A **84**, 042101 (2011).
[6] Y.-L. Wang, H. Jiang, and H.-S. Zong, Phys. Rev. A **96**, 022116 (2017).
[7] Y.-L. Wang, M.-Y. Lai, F. Wang, H.-S. Zong, and Y.-F. Chen, Phys. Rev. A **97**, 042108 (2018).
[8] H. Aoki, M. Koshino, D. Takeda, H. Morise, and K. Kuroki, Phys. Rev. B **65**, 035102 (2001).
[9] C. Ortix and J. van den Brink, Phys. Rev. B **81**, 165419 (2010).
[10] A. del Campo, M. G. Boshier, and A. Saxena, Sci. Rep. **4**, 5274 (2014).
[11] Y.-L. Wang, G.-H. Liang, H. Jiang, W.-T. Lu, and H.-S. Zong, J. Phys. D: Appl. Phys. **49**, 295103 (2016).
[12] W.-R. Cao, Y.-L. Wang, X.-L. Chen, H. Jiang, C.-T. Xu, and H.-S. Zong, Phys. Lett. A **383**, 2124 (2019).
[13] M.-Y. Lai, Y.-L. Wang, G.-H. Liang, and H.-S. Zong, Phys. Rev. A **100**, 033825 (2019).
[14] C. Ortix, J. W. F. Venderbos, R. Hayn, and J. van den Brink, Phys. Rev. B **89**, 121408(R) (2014).
[15] N. P. Armitage, E. J. Mele, and A. Vishwanath, Rev. Mod. Phys. **90**, 015001 (2018).
[16] A. Szameit, F. Dreisow, M. Heinrich, R. Keil, S. Nolte, A. Tünnermann, and S. Longhi, Phys. Rev. Lett. **104**, 150403 (2010).
[17] R. Spittel, P. Uebel, H. Bartelt, and M. A. Schmidt, Opt. Express **23**, 12174 (2015).
[18] R. C. T. da Costa, Phys. Rev. A **25**, 2893 (1982).
[19] M. Encinosa and B. Etemadi, Phys. Rev. A **58**, 77 (1998).
[20] M. Encinosa and L. Mott, Phys. Rev. A **68**, 014102 (2003).
[21] J. Gravesen and M. Willatzen, J. Math. Phys. **46**, 012107 (2005).
[22] G. Ferrari and G. Cuoghi, Phys. Rev. Lett. **100**, 230403 (2008).
[23] B. Jensen and R. Dandoloff, Phys. Rev. A **80**, 052109 (2009).
[24] C. Ortix and J. van den Brink, Phys. Rev. B **83**, 113406 (2011).
[25] G. de Oliveira, J. Math. Phys. **55**, 092106 (2014).
[26] T. Kosugi, J. Phys. Soc. Jpn. **80**, 073602 (2011).
[27] O. Kenneth and J. E. Avron, Ann. Phys. **349**, 325 (2014).
[28] Y.-L. Wang, L. Du, C.-T. Xu, X.-J. Liu, and H.-S. Zong, Phys. Rev. A **90**, 042117 (2014).
[29] S. Matsutani, Phys. Rev. A **47**, 686 (1993).
[30] M. Burgess and B. Jensen, Phys. Rev. A **48**, 1861 (1993).
[31] F. T. Brandt and J. A. Sánchez-Monroy, Phys. Lett. A **380**, 3036 (2016).
[32] Z. Q. Yang, X. Y. Zhou, Z. Li, W. K. Du, and Q. H. Liu, Phys. Lett. A **384**, 126604 (2020).
[33] O. Parrikar, T. L. Hughes, and R. G. Leigh, Phys. Rev. D **90**, 105004 (2014).
[34] H. Taira and H. Shima, J. Phys.: Condens. Matter **22**, 075301 (2010).
[35] W. Beugeling, A. Quelle, and C. Morais Smith, Phys. Rev. B **89**, 235112 (2014).
[36] N. Zhao, H. Dong, S. Yang, and C. P. Sun, Phys. Rev. B **79**, 125440 (2009).
[37] J. F. O. de Souza, C. A. de Lima Ribeito, and C. Furtado, Eur. Phys. J. B **90**, 98 (2017).
[38] F. T. Brandt and J. A. Sánchez-Monroy, Europhys. Lett. **111**, 67004 (2015).
[39] H. Taira and H. Shima, J. Phys. A: Math. Theor. **43**, 354013 (2010).
[40] P. A. M. Dirac, Proc. R. Soc. London Ser. A **133**, 60 (1931).
[41] T. T. Wu and C. N. Yang, Phys. Rev. D **12**, 3845 (1975).
[42] S. Nishino, R. Matsudo, M. Warschinke, and K.-I. Kondo, Prog. Theor. Exp. Phys. **2018**, 103B04 (2018).
[43] S. Deguchi and K. Fujikawa, Phys. Lett. B **802**, 135210 (2020).
[44] G.'t Hooft, Nucl. Phys. B **79**, 276 (1974).
[45] K.-I. Kondo, Phys. Lett. B **762**, 219 (2016).
[46] P. San-Jose, J. González, and F. Guinea, Phys. Rev. Lett. **108**, 216802 (2012).
[47] A. Uri, Y. Kim, K. Bagani, C. K. Lewandowski, S. Grover, E. O. Auerbach, Nadav Lachman, Y. Myasoedov, T. Taniguchi, K. Watanabe, J. Smet, and E. Zeldov, Nat. Phys. **16**, 164 (2020).
[48] S. K. Donaldson and P. B. Kronheimer, *The Geometry of Four-Manifolds* (Oxford University Press, Oxford, 1990).
[49] G.-H. Liang, Y.-L. Wang, M.-Y. Lai, H. Zhao, H.-S. Zong, and H. Liu, Phys. Rev. A **101**, 053632 (2020).
[50] Y.-L. Wang, H.-S. Zong, H. Liu, and Y.-F. Chen, Phys. Rev. B **102**, 155153 (2020).
[51] D.-B. Zhang, G. Seifert, and K. Chang, Phys. Rev. Lett. **112**, 096805 (2014).
[52] X. Tan, D.-W. Zhang, W. Zheng, X. Yang, S. Song, Z. Han, Y. Dong, Z. Wang, D. Lan, H. Yan, S.-L. Zhu, and Y. Yu, Phys. Rev. Lett. **126**, 017702 (2021).
[53] W. Beugeling, Phys. Rev. B **104**, 115428 (2021).
[54] C. L. Kane and E. J. Mele, Phys. Rev. Lett. **95**, 226801 (2005).
[55] C. L. Kane and E. J. Mele, Phys. Rev. Lett. **95**, 146802 (2005).
[56] B. A. Bernevig and S.-C. Zhang, Phys. Rev. Lett. **96**, 106802 (2006).
[57] B. A. Bernevig, T. L. Hughes, and S.-C. Zhang, Science **314**, 1757 (2006).
[58] M. Z. Hasan and C. L. Kane, Rev. Mod. Phys. **82**, 3045 (2010).
[59] X.-L. Qi and S.-C. Zhang, Rev. Mod. Phys. **83**, 1057 (2011).

[60] M. A. Olpak, Mod. Phys. Lett. A **27**, 1250016 (2012).
[61] K. Flouris, M. M. Jimenez, and H. J. Herrmann, Phys. Rev. B **105**, 235122 (2022).
[62] R. A. Bertlmann, *Anomalies in Quantum Field Theory* (Clarendon, London, 1996).
[63] H. Zhao, Y.-L. Wang, C.-Z. Ye, R. Cheng, G.-H. Liang, and H. Liu, Phys. Rev. A **105**, 052220 (2022).
[64] M. Encinosa, L. Mott, and B. Etemadi, Phys. Scr. **72**, 13 (2005).
[65] A. P. Korte and G. H. M. van der Heijden, J. Phys.: Condens. Matter **21**, 495301 (2009).
[66] W. Beugeling, N. Goldman, and C. M. Smith, Phys. Rev. B **86**, 075118 (2012).
[67] Y. Liu, L.-R. Ding, A.-L. He, and Y.-F. Wang, J. Phys.: Condens. Matter **32**, 505501 (2020).
[68] J. Ningyuan, C. Owens, A. Sommer, D. Schuster, and J. Simon, Phys. Rev. X **5**, 021031 (2015).